DEVELOPMENTS FOR THE HIGH FREQUENCY POWER TRANSFORMER DESIGN AND IMPLEMENTATION

Mika Sippola

DEVELOPMENTS FOR THE HIGH FREQUENCY POWER TRANSFORMER DESIGN AND IMPLEMENTATION

Mika Sippola

Dissertation for the degree of Doctor of Science in Technology to be presented with due permission for public examination and debate in Auditorium S4 at Helsinki University of Technology (Espoo, Finland) on the 13th of June, at 12 o'clock noon.

Helsinki University of Technology

Department of Electrical and Communications Engineering

Applied Electronics Laboratory

Teknillinen Korkeakoulu

Sähkö- ja tietoliikennetekniikan osasto

Sovelletun Elektroniikan laboratorio

ABSTRACT

In this thesis design and manufacturing of ferrite based high frequency power transformers is considered. The primary aim of the work was to study core and winding losses and in particular thermal modeling of high frequency power transformers and to determine appropriate loss and temperature rise modeling methods for power converter applications. The secondary aim of the work was to study improved, mass manufacturable winding methods for toroidal, tube-type planar and disc-type planar high frequency power transformers.

The thesis consists of 7 publications and a summary with conclusions. In summary high frequency power transformers, their losses, temperature rise and winding parasitics are illustrated and discussed. In [P1] the DC/DC converter technology for distributed microprocessor and telecom power systems was reviewed from literature. In [P2] the analytical high frequency power transformer design equations for core and winding losses and transformer temperature rise were reviewed from literature, formulated for spreadsheet type calculations using excitation, material, geometry and winding implementation parameters and validated by in circuit temperature rise comparisons between calculated and measured values using regression analysis. In [P3] thermal and electromagnetic compatibility (EMC) performance of seven printed circuit board (PCB) options were studied experimentally. In papers [P4],[P5],[P6] and [P7] new manufacturing methods were developed for toroidal, tube and disc-type transformer geometries.

In literature review [P1] the power density of commercial DC/DC converters was found to increase versus increasing output power only suggesting that these tend to have a fixed (34 cm^3 / 2 inch^3) industry standard minimum volume. On the other hand in journal and conference papers much wider range of power densities have been reported (max. 7.75 W/cm^3 / 130 W/inch^3).The tube-type planar transformer geometry was found to provide more potential for low profile, high power density transformers over disc-type planar transformers. A single toroidal core is not suitable for low profile, high power density transformers due to dimensional constraints. In [P2] the core and winding loss calculation methods in literature were found to provide appropriate accuracy for the practical design purposes. Thermal test block tests suggested a slight modification (multiplier 2 x) for analytical convective heat transfer equation from the literature [34]. The results from in circuit temperature rise comparisons suggest that the transformer total losses can be predicted with the average standard error below 0.2W with datasheet type information only. Further, if conductive thermal resistance from transformer via printed circuit board substrate to ambient is available the transformer operating temperature could be predicted with appropriate accuracy (5.6ºC) as well. Losses in interconnecting wires was the biggest uncertainty of in-circuit transformer temperature rise estimations. In [P3] the thermal resistance from surface mounted component on each Printed Circuit Board to ambient varied from 58.7˚K/W (1-layer FR4 0.38$) to 7.9˚K/W (2-layer IMS 2.15$) corresponding to approximately 2.7 times difference in throughput power for the same (100˚K) temperature rise when resistive-type (P = I^{2}R) losses are assumed. In [P4] the static shield and windings of common mode choke were successfully deposited and etched directly on the toroidal NiZn core and transfer loss resonant frequency above 1.2GHz was achieved. In [P5] multilayer foil winding with interleaved primary and secondary layers was successfully implemented for EFD30-type transformer using the new manufacturing method resulting leakage inductance to be 10% of the value achieved using a wire-wound winding. The increase of winding losses with wire-wound version was 6.2 times higher than with the proposed winding method across the frequency range of 100kHz - 1.6MHz. In [P6] new winding layout principles for Z-folded inductive components were developed. As a results a single sided FLEX can be used in order to for reduce material costs and to make level of interleaving between primary and secondary windings adjustable. Copper thickness doubling and adjacent FLEX face via forming techniques were also developed. In [P7] it was found that the 1-pole (ER25) core with widest conductor resulted lowest total losses but with 2-pole transformer the minimum losses are achieved with the least number of FLEX segments and these may be preferred when cost – performance is considered.

Keywords – High frequency power transformers, transformer design, transformer manufacturing, core loss modeling, winding loss, winding AC-resistance, thermal modeling, natural convection, planar transformer, toroidal winding, Z-folded winding

PREFACE

CONTENTS

LIST OF PUBLICATIONS

This thesis is based on the following publications:

[P1] Sippola M., Sepponen R. "DC/DC Converter Technology for distributed power systems - a literature review", *IEEE Aerospace and Electronic Systems Magazine,* (Submitted) / Applied Electronics Laboratory Reseach Report (optionally)

[P2] Sippola M., Sepponen R., "Accurate prediction of High Frequency Power Transformer Losses and Temperature rise", *IEEE Transactions on Power Electronics*, vol. 17, no. 5, September 2002

[P3] Sippola M., von Rauner T., Siren H., Sepponen R., "The Effect of Printed Circuit Board on Cooling and EMC of Switched Mode Power Supply", *Proceedings of 2000 IEEE 31st Annual Power Electronics Specialists Conference (PESC00)*, vol. 3, pp.1267 - 1272, 18 - 23 June 2000, Galway, Ireland

[P4] Sippola M., Siren H., "New winding method for common mode choke", *Proceedings of 1998 6th Biennal Conference on Electronics and Microsystems Technology (BEC'98)* , pp. 49 - 52, October 7 - 9 1998, Tallinn, Estonia

[P5] Sippola M., Sepponen R. ,"A Manufacturing Method for Multilayer tube winding with interleaved primary and secondary windings", *Proceedings of 15th Annual IEEE Applied Power Electronics Conference and Exposition*, vol. 2, pp. 787 - 790, 6 - 10 February 2000, New Orleans, Louisiana

[P6] Sippola M., Sepponen R., "Reel-to-reel manufacturable, low cost, high performance Z-folded planar inductive components technology", IEEE Transactions on Electronics Packaging Manufacturing, (Submitted - in Review)

[P7] Sippola M., Sepponen R. ,"Design for Manufacturing considerations for Z-folded planar transformers", IEEE Transactions on Magnetics, (Submitted) / Electronics Letters (Submitted) / Applied Electronics Laboratory Reseach Report (optionally)

NOMENCLATURE

a = winding window dimension
a_{th} = coefficient of thermal model
A = area
A_c = core area
A_{prim} = primary winding area
A_{sec} = secondary winding area
A_w = winding area
b = winding window dimension
b_{th} = coefficient of thermal model
B = flux density
$\hat{B}$ = peak flux density
B_{max} = maximum flux density
B_{min} = minimum flux density
c = core dimension
ct = core hysteresis loss temperature coefficient
ct_1 = core hysteresis loss temperature coefficient
ct_2 = core hysteresis loss temperature coefficient
c_{th} = coefficient of thermal model
C_{layer} = capacitance between winding layers
C_{prim} = primary intrawinding capacitance
C_{prim_sec} = primary to secondary capacitance
C_{sec} = secondary intrawinding capacitance
C_{total} = total capacitance
d = core dimension
d_{foil} = foil thickness
d_{th} = coefficient of thermal model
d_{wire} = wire diameter
D = duty cycle
e_{th} = coefficient of thermal model
f = frequency
f_{eq} = equivalent frequency
h = harmonic index
h_{obj} = height of object
I_p = primary rms current
I_{ph} = primary rms current at h'th harmonic frequency
I_s = secondary rms current
k = time instant index
K = number of sub periods in total switching period
K_1 = core hysteresis loss coefficient
K_2 = core hysteresis loss coefficient
K_3 = core hysteresis loss coefficient
l_{obj} = length of object
l_c = core length
l_w = average winding turn length
L_{layer} = inductance of volume between winding layers
L_{leak_prim} = primary leakage inductance
L_{leak_sec} = secondary leakage inductance
L_m = magnetizing inductance
$L_{section}$ = inductance of a section
L_{total} = inductance of total winding
m = number of layers in winding section
n = ratio of primary winding area to total winding area
N = number of turns per layer
N_{prim} = number of primary turns
N_s = number of sections
N_{sec} = number of secondary turns
p_{eddy} = eddy current core loss density

p_{hyst} = hysteresis core loss density
$P_{conduction}$ = Conductive heat transfer capacity
$P_{convection}$ = convective heat transfer capacity
P_{cu} = winding (copper) loss
P_{eddy} = eddy current core loss
P_{fe} = core (ferrite) loss
P_{hyst} = hysteresis core loss
P_m = magnetizing current winding loss
$P_{radiation}$ = radiative heat transfer capacity
$P_{winding}$ = winding loss
r_c = core area radius
r_w = winding area radius
R_{ac} = AC-resistance
R_{dc} = DC-resistance
(R_{ac}/R_{dc}) = ratio of AC and DC resistance
R_{core} = core loss resistance
R_{prim} = primary resistance
R_{sec} = secondary resistance
$R_{th\_obj\text{-}PCB}$ = conductive thermal resistance from object to Printed Circuit board (PCB)
t = time
T = temperature
T_{amb} = ambient temperature
T_{cu} = copper temperature
T_{fe} = ferrite temperature
T_{obj} = object temperature
T_{pcb} = Printed Circuit Board (PCB) temperature
U_{in} = input voltage
w = winding layer width
w_{obj} = width of object
x = distance between winding layers
y = ratio of foil thickness and skin depth
α = copper fill factor
β = convective heat transfer coefficient
ε = emissivity
ε_o = vacuum permittivity
ε_r = relative permittivity
ξ = ratio of wire diameter to skin depth $\left(\cdot \frac{\sqrt{2}}{\pi}\right)$
σ = resistivity of winding material
σ_B = Boltzmann coefficient
σ_p = resistivity of primary winding material
σ_s = resistivity of secondary winding material
δ = skin depth
ω = angular frequency
μ_0 = permeability of vacuum
μ_r = relative permeability
ρ = effective resistance of ferrite
τ = switching period
EMI = ElectroMagnetic Interference
FEM = Finite Element Method
AC = Alternating Current
DC = Direct Current
VRM = Voltage Regulation Module
PCB = Printed Circuit Board
IMS = Insulated Metal Substrate
NiZn = Nickel Zinc (ferrite)
MnZn = Manganeze Zinc (ferrite)
HDI = High Density Interconnected
PWM = Pulse Width Modulated
EMC = Electromagnetic Compatibility
FLEX = FLEXible Circuit board

1 INTRODUCTION

1.1 BACKGROUND

Power transformers are usually considered as the bulkiest and most expensive components in a switched mode power supply. They are also critical for power converter performance: dynamic response, efficiency, cross regulation between multiple secondaries and electromagnetic interference (EMI). Suitable power transformers are seldom available as standard components and they must be specified and designed during the converter design process. High frequency (>50Hz, typ. 1kHz - 1MHz) power transformer design (i.e. analysis of losses and temperature rise) has attained considerable attention in literature as well. For example, core losses have been modeled using Steinmetz equation [1],[2],[3],[4], additional harmonic analysis [5] and form factor correction [6] while winding losses have been modeled using DC-resistance [1], analytical expressions for winding AC resistance (R_{ac}/R_{dc}) [2], [6], [5], [4], [3] or Finite Element Method (FEM) derived winding AC resistance (R_{ac}/R_{dc}) factor [7]. Heat transfer has been modeled as a constant thermal resistance [2],[5],[3] or as a non-linear heat transfer coefficient [4]. However, it is also claimed that despite the much work on high frequency power transformer modeling and design the accuracy of the proposed design methods and appropriate modeling detail level is difficult to judge due to limited experimental verification [8]. It is also suggested that such validation should be based on a comparison between calculated and measured temperature rise values but remarked that this is seldom considered in the literature. This may relate into the difficulties involved in the accurate thermal characterization and in particular to the determination of convective heat transfer coefficient [4].

On the other hand although the theoretical transformer power density studies based on loss and temperature rise constraints [9],[10],[11],[12],[13],[14],[15] have reached transformer throughput power densities of 358W/cm^3 [12] the values obtained in reality are limited by the fabrication technique constraints [9]. *Solid wire winding* is propably the most commonly used winding method but it's high frequency losses and leakage inductance have become a problem in high frequency power conversion. The prior can be reduced by using *litz wire winding* but this increases material and manufacturing costs. The latter can be reduced by using interleaving between primary and secondary windings, but this also makes manufacturing more complicated. With *foil conductors* the skin effect can be minimized and high frequency winding losses can be reduced with optimum conductor thickness selection [16]. Foil conductor has also potential for higher copper fill factor than litz wire. However, the restrictions in manufacturing methods have restricted the use of interleaving with foil windings in order to reduce leakage inductance and proximity effect [9]. The planar transformers [17] have also gained popularity in order to meet low profile and/or high current requirements of telecom and microprocessor voltage regulation modules (VRM), as an example. The use of multilayer *printed circuit board* traces for planar windings is an optimum solution if assembly is considered. Interleaving [18] between primary and secondary windings can also be easily utilized and the parasitics will be reproduced within the printed circuit board (PCB) manufacturing tolerances. The low copper fill factor of standard FR4 PCB (typ. 0.2 - 0.3) may result low power conversion efficiency while the use of non-standard copper thickness may yield prohibitive costs particularly if buried vias are used [19]. *Stacked copper stampings* can be used for producing a high copper fill factor planar winding. Assembly of insulation layers and soldered connections between winding layers makes mass manufacturing process more difficult, however [17],[20]. *Z-folded* winding uses accordion (i.e. zig-zag) folded flexible circuit board to build up a multilayer planar winding structure [21],[22]. Although such winding has inherent vias between winding layers some soldering operations are usually needed for terminations and to connect layers reliable. All this makes manufacturing process more complicated. *Thick film* [23],[24] and *thin film* [25],[26] manufacturing methods have also been employed in manufacture of low profile, high power density inductive components. Poor material characteristics of screen printed ferrites, deposited copper, conductive silver paste etc. with non-optimum flat planar transformer geometry results low power conversion efficiency (75%[23], 43.4%[27]), however. *High density interconnection* (HDI) process can utilize optimum materials for core and winding resulting high efficiency and high power density low profile inductive components and has been used in aerospace applications [28].

1.2 OBJECTIVES OF THE STUDY

It can be concluded that successful utilization of high frequency power transformer requires not only appropriate modeling of core and winding losses and temperature rise but also efficient and mass manufacturable methods to implement windings. In this thesis both design and implementation of high frequency power transformers are considered.

- The primary aim of the work was to study core and winding losses and in particular temperature rise of high frequency power transformers, to determine appropriate loss and temperature rise *modeling methods* and detail levels for power converter applications and to determine the accuracy of resulting loss and temperature rise calculation algorithm by temperature rise comparisons as suggested in [8].

- The secondary aim of the work was to develop improved, mass manufacturable winding *implementation methods* for toroidal, tube-type planar and disc-type planar high frequency power transformers and to validate them by calculations and measurements.

In this work standard materials (ferrite core and copper windings) are considered. Amorphic core materials show promising performance in terms of saturation flux density and core loss but are limited into toroidal core shapes at the moment. Switching frequency range of 100 - 300 kHz is considered as in many cases the power semiconductor switching losses limit the switching frequency around such figures in order to achieve acceptable converter efficiency.

1.3 CONTENTS OF THE THESIS

This thesis consists of 7 publications and a summary with conclusion. In summary high frequency power transformers, their losses, temperature rise and winding parasitics are illustrated and discussed. The aim of the summary is also to emphasize relationships between theoretical design calculations and practical transformer manufacturing issues more than what was done in the separate papers. The manufacturing details and measurement methods used for example to verify loss calculations are considered in more detail in the separate papers only.

In [P1] the DC/DC converter technology for distributed microprocessor and telecom power systems was reviewed with the focus on application requirements, topologies, components and packaging. The DC/DC converter power densities reported in the literature were compared with the values of commercial DC/DC converters.

In [P2] the analytical high frequency power transformer design equations for core and winding losses and transformer temperature rise were reviewed from literature and formulated for spreadsheet type calculations using excitation, material, geometry and winding implementation parameters. Such formulation is intented for power density driven, manufacturing constrained transformer design optimization. Considerable effort was put into empirical validation of the derived loss and temperature rise calculations. A calorimeter was build for core loss measurements under DC/DC-converter exitation in order to verify calculated core loss values. FEM analysis was used for verifying the analytical winding AC-resistance calculations. Thermal test blocks were used for verifying the analytical heat transfer equations for convective and radiative heat transfer. An empirical thermal model was also developed for EFD20-type transformer using DC-current induced core and winding losses in order to validate loss calculations in actual circuit operation accurately. As a final figure-of-merit the transformer temperature rise values predicted by the developed design spreadsheet were compared with the values measured in circuit operation using regression analysis.

In [P3] thermal and electromagnetic compatibility (EMC) performance of seven printed circuit board (PCB) options (1-layer FR4, 2-layer FR4, 4-layer FR4, 1-layer IMS, 2-layer IMS, 1-layer 0.1mm FR4 and 2-layer 0.1mm FR4) were studied experimentally. Although the main consideration in the paper is on the EMC issues the value of thermal resistance from component via substrate to ambient is needed in power transformer temperature rise calculations.

In papers [P4],[P5],[P6] and [P7] new manufacturing methods were developed for toroidal, tube and disc-type transformer geometries. In [P4] a toroidal winding manufacturing method based on direct copper plating and etching on NiZn core is presented and validated using FEM analysis and impedance analyzer measurements. Although the paper considers a common mode choke and in particular interwinding capacitance the manufacturing method itself can be extended for signal and power transformers as well. The proposed manufacturing method is suitable for batch type processing where hundreds or thousands of components are processed simultaneously. In [P5] a new multilayer tube-type winding manufacturing method with inherent interleaving between primary and secondary winding layers is presented, analyzed and validated with measurements. In [P6] a reel-to-reel mass manufacturable, leadless surface mounted Z-folded planar transformer concept is presented with the winding layout principles for integral terminations, effective copper thickness doubling, inherent via forming between the winding layers and flexible interleaving. The paper [P7] presents a more detailed manufacturability – electrical performance analysis and comparison of z-folded transformer options.

2 POWER TRANSFORMERS

With electrical transformer energy is transferred between primary and secondary circuits via inductive coupling. A transformer equivalent circuit (Figure 1) consists of: ideal transformer (N_{prim}, N_{sec}), loss components (R_{prim}, R_{sec}, R_{core}), magnetizing inductance (L_m) and parasitic components (L_{leak_prim}, L_{leak_sec}, C_{prim}, C_{sec}, $C_{prim-sec}$). The (linear) equivalent circuit is not sufficient for switched mode power supply transformer design analysis with non-sinusoidal currents and voltages. In following linear models are used for parasitic components and magnetization inductance only while the losses are calculated directly from the winding and core material properties, transformer geometry and electrical exitation.
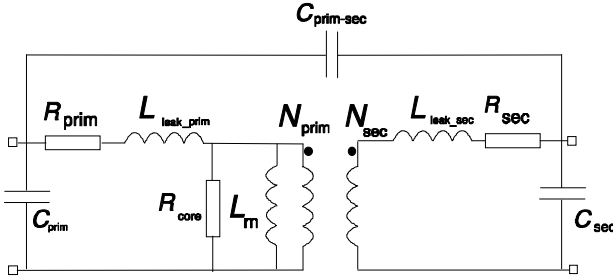

Figure 1: 2-winding transformer equivalent circuit

where
N_{prim} = number of primary turns
N_{sec} = number of secondary turns
R_{core} = core loss resistance
R_{prim} = primary resistance
R_{sec} = secondary resistance
L_m = magnetizing inductance
L_{leak_prim} = primary leakage inductance
L_{leak_sec} = secondary leakage inductance
C_{prim} = primary intrawinding capacitance
C_{prim_sec} = primary to secondary capacitance
C_{sec} = secondary intrawinding capacitance

2.1 TRANSFORMER GEOMETRIES

A general inductive component (Figure 2) consists of a winding (typ. of copper) interlinked with a core (typ. of high permeability material). Also, the winding passes around the core area A_c resulting winding length l_w. Similarly, the core passes around winding area A_w resulting core length l_c.
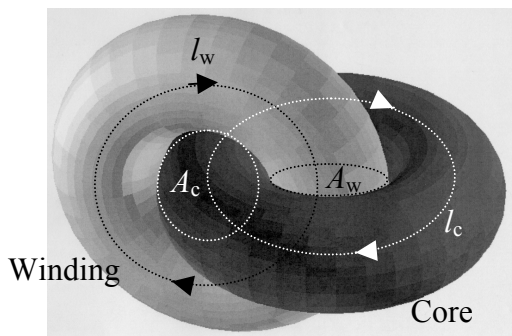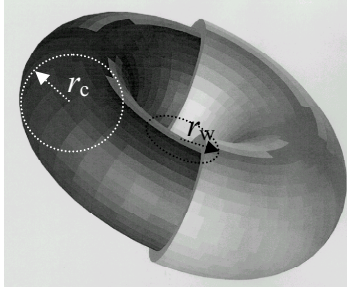

Figure 2: Geometrical parameters of a general inductive component

where
A_c = core area
A_w = winding area
l_c = core length
l_w = average winding turn length

In a physical inductive component the relation between the geometrical parameters is determined by the component geometry and dimensions (Figure 3).

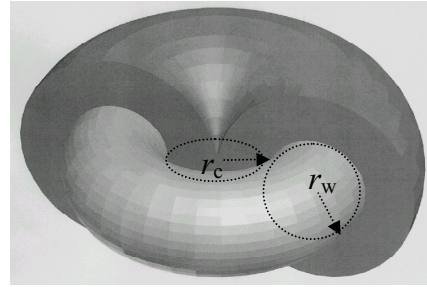Toroidal core geometry (half of winding is cut away)

$$A_c = \pi r_c^2$$
$$l_c = 2\pi(r_w + r_c)$$
$$A_w = \pi r_w^2$$
$$l_w = \pi(2r_c + r_w)$$

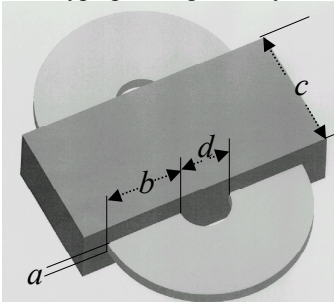Pot-core geometry (half of core is cut away)

$$A_c = \pi r_c^2$$
$$l_c = \pi(2r_w + r_c)$$
$$A_w = \pi r_w^2$$
$$l_w = 2\pi(r_c + r_w)$$

Disc-type planar geometry

$$A_c = c \cdot d$$
$$l_c = 2a + 2b + \frac{5}{2}d$$
$$A_w = a \cdot b$$
$$l_w = 4b + 2c + 2d$$

Tube-type planar geometry
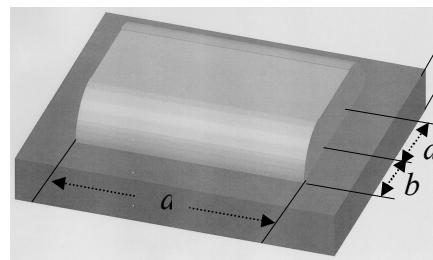
$$A_c = c \cdot d$$
$$l_c = 2a + 2b + 2d$$
$$A_w = a \cdot b$$
$$l_w = 4b + 2c + 2d$$

Figure 3: Basic transformer geometries

where r_c = core area radius
r_w = winding area radius
a = winding window dimension
b = winding window dimension
c = core dimension
d = core dimension

2.2 WINDING IMPLEMENTATION METHODS

Power transformer winding implementation methods discussed in Introduction are illustrated in Figure 4 below.
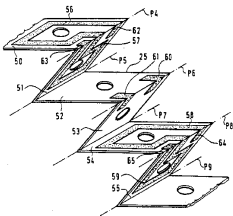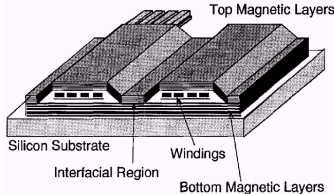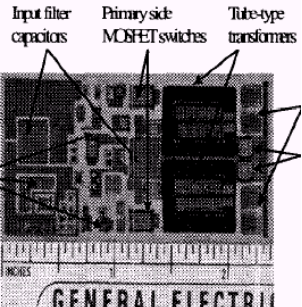
SOLID WIRE	FOIL	MULTILAYER PCB	STAMPING
[P5]	[P5]	[Lucent Technologies]	[Payton]

Z-FOLDED	INTEGRATED	HDI
[Alcatel Converters]	[26]	[28]

Figure 4: Winding implementation methods

3 POWER TRANSFORMER DESIGN

This thesis considers power transformer design as calculation of core and winding losses in order to determine power transfer efficiency a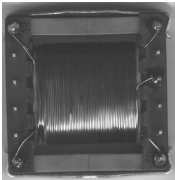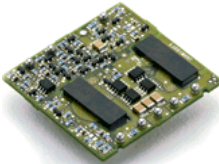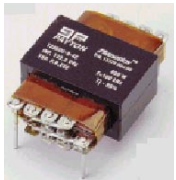nd temperature rise. Winding parasitics are also briefly considered. Transformer core and winding loss calculations are considered in a case where magnetization and total load current in windings doesn't have a DC-component i.e. for example a push-pull type converter topology with symmetrical secondary. Such operation results lowest core losses and is preferred for highest efficiency. A DC-component in magnetizing current causes increase in hysteresis core losses and would require additional experimental correction factors to be determined [29] while non-symmetrical loading of secondary(ies) would invalidate winding AC-resistance and loss analysis according to [30]. Magnetic skin depth in core is neglected and constant flux density in core is assumed due to relatively low operating frequency range (100kHz - 300kHz) considered in this work.

3.1 HYSTERESIS CORE LOSSES

In ferro- and ferrimagnetic materials the net magnetization is coverned by the wall movements (Figure 5) of highly non-uniform and saturated ~μm dimension magnetic domains (Bloch domains) [31]. The losses associated with the domain wall movements under cyclical magnetization are called hysteresis losses. Hysteresis losses are increased for example by mechanical voids and impurities due to energy associated with rapid domain wall movements (Barkhausen-jumps) to overcome these barriers [32].
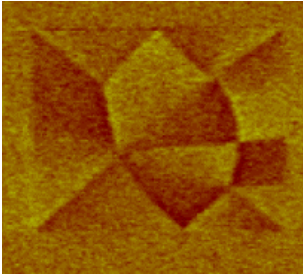
Figure 5a: Magnetic domains in magnetic force microscopy image of 3 x 3μm permalloy element [33]
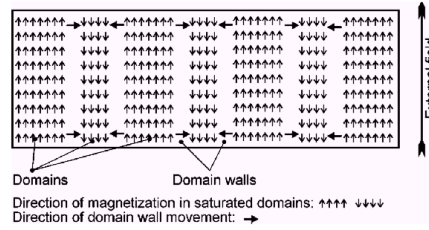
Figure 5b: Illustrated domain wall movements during magnetization [29]

Hysteresis loss density with sinusoidal exitation without a DC-component can be modeled with Steinmetz equation [34]:

$$p_{\text{hyst}} = K1 \cdot f^{K2} \cdot \hat{B}^{K3} \left(ct_2^2 T - ct_1 T + ct \right) \tag{1}$$

where
p_{hyst} = hysteresis core loss density (W/m^3)
$K1, K2, K3$ = loss coefficients
ct, ct_1, ct_2 = temperature coefficients
T = temperature (°K / ˚C)
f = frequency (Hz)
$\hat{B}$ = peak flux density (T)

Loss coefficients (K1, K2 and K3) or equivalent loss density graphs are provided by ferrite manufacturers usually for sinusoidal excitation only. To scope with arbitrary exitation waveforms the concept of equivalent frequency based on the weighted average remagnetization velocity can be used [35]:

$$p_{\text{hyst}} = \frac{1}{\tau} \cdot K1 \cdot f_{\text{eq}}^{K2-1} \cdot \hat{B}^{K3} (ct_2 T^2 - ct_1 T + ct) \tag{2}$$

where
τ = switching period (s)
f_{eq} = equivalent frequency (Hz)

$$f_{eq} = \frac{2}{\pi^2} \sum_{k=2}^{K} \left(\frac{B_k - B_{k-1}}{B_{\max} - B_{\min}} \right)^2 \cdot \frac{1}{t_k - t_{k-1}} \tag{3}$$

where $\quad B_{max}$ = maximum flux density during switching period (T)
$\quad\quad\quad\quad\quad B_{min}$ = minimum flux density during switching period (T)
$\quad\quad\quad\quad\quad B_k$ = flux density at t_k (T)
$\quad\quad\quad\quad\quad t_k$ = time instant k (s)
$\quad\quad\quad\quad\quad K$ = number of sub periods in switching period

For pulse width modulated (PWM) DC/DC converter (3) reduces into:

$$f_{eq} = \frac{2}{\pi^2} f \frac{1}{D(1-D)} \tag{4}$$

where $\quad\quad\quad D$ = duty cycle

As an example, for an active clamp forward converter, the peak flux density is:

$$\hat{B} = \frac{1}{2} \frac{U_{in}D}{fN_{prim}A_c} \tag{5}$$

where $\quad\quad\quad U_{in}$ = input voltage (V)
$\quad\quad\quad\quad\quad A_c$ = Core area (m^2)
$\quad\quad\quad\quad\quad N_{prim}$ = number of primary turns

The total hysteresis core loss P_{hyst} is calculated by multiplying the core hysteresis loss density (2) by core volume:

$$P_{hyst} = \frac{1}{\tau} K1 \left(\frac{2}{\pi^2} f \frac{1}{D(1-D)} \right)^{K2-1} \left(\frac{1}{2} \frac{U_{in}D}{fN_{prim}A_c} \right)^{K3} (ct_2 T^2 - ct_1 T + ct) \cdot A_c l_c \tag{6}$$

where $\quad\quad\quad l_c$ = Core length (m)

3.2 EDDY CURRENT CORE LOSSES

Due to finite resistivity of core material eddy currents are induced into the transformer core by the changing magnetic flux (Figure 6). In order to reduce such losses ferrites consist (Figure 7) of semi conducting (0.001Ωm MnZn, 30Ωm NiZn) grain crystallites isolated by a thin isolating layer. Bulk resistivity and permittivity of ferrites is thus strongly dependent on the frequency and temperature as the isolation and grain resistances become bypassed by the capacitances between and inside the grains or reduces as frequency or temperature increases, respectively. For example, in [34] measured bulk resistivity and relative permittivity of 3F3 type ferrite varied from 0.3 to 2.1Ωm and 110000 to 60000 within frequency and temperature ranges of 10kHz - 1MHz and 25˚C - 100˚C, respectively.
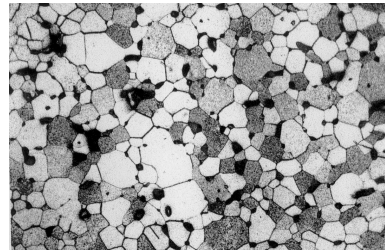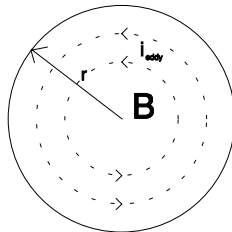

Figure 6: Eddy currents in conducting cylinder Figure 7: Microstructure of MnZn ferrite [31, p.124]

When cylinder geometry with uniform flux density and negligible magnetic field generated by eddy current is assumed the eddy current core loss density is [34],[36]:

$$p_{\text{eddy}} = \frac{\pi}{4\rho}(f\hat{B})^2 A_{\text{c}} \tag{7}$$

where $\qquad p_{\text{eddy}}$ = eddy current loss density (W/m^3)
$\qquad\qquad\quad \rho$ = effective resistance of ferrite (Ωm)

Using (5) and multiplying core eddy current loss density by core volume results total eddy current loss P_{eddy} (W):

$$P_{\text{eddy}} = \frac{\pi}{4\rho}\left(\frac{U_{\text{in}}D}{2N_{\text{prim}}}\right)^2 l_{\text{c}} \tag{8}$$

Regression analysis between calorimetric core loss measurements and values calculated according to (6) and (8) using ferrite loss coefficients and resistivity provided by manufacturer [34] in Figure 8 shows good agreement between theory and experiments (y = 1.0372x - 0.0174: r^2 = 0.9861). Magnetizing current winding loss was neglected in the calculations.

Core losses

y = 1,0372x - 0,0174
R^2 = 0,9861
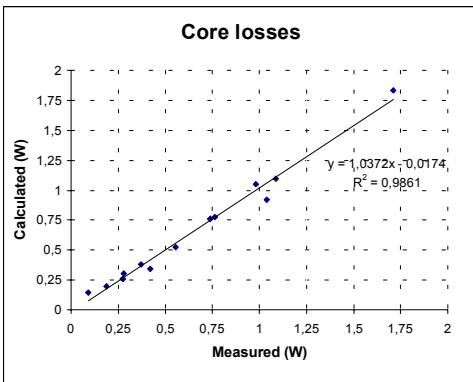
Figure 8: Comparison of measured and calculated core losses (6),(8)

3.3 LOAD CURRENT WINDING LOSSES

Winding loss P_{winding} of two winding transformer is

$$P_{\text{winding}} = I_{\text{p}}^2 R_{\text{prim}} + I_{\text{s}}^2 R_{\text{sec}} \tag{9}$$

where $\qquad I_{\text{p}}$ = primary rms current (A)
$\qquad\qquad\quad I_{\text{s}}$ = secondary rms current (A)
$\qquad\qquad\quad R_{\text{prim}}$ = primary resistance (Ω)
$\qquad\qquad\quad R_{\text{sec}}$ = secondary resistance (Ω)

The DC-resistance of primary R_{prim} and secondary R_{sec} winding can be expressed as

$$R_{\text{prim}} = \sigma_{\text{p}}\frac{l_{\text{w}}N_{\text{prim}}^2}{A_{\text{prim}}} \tag{10}$$

$$R_{\text{sec}} = \sigma_{\text{s}}\frac{l_{\text{w}}N_{\text{sec}}^2}{A_{\text{sec}}} \tag{11}$$

where $\qquad \sigma_{\text{p}}$ = resistivity of primary winding material (Ωm)
$\qquad\qquad\quad \sigma_{\text{s}}$ = resistivity of secondary winding material (Ωm)
$\qquad\qquad\quad l_{\text{w}}$ = average length of winding turn (m)
$\qquad\qquad\quad A_{\text{prim}}$ = primary winding area (m^2)
$\qquad\qquad\quad A_{\text{sec}}$ = secondary winding area (m^2)
$\qquad\qquad\quad N_{\text{prim}}$ = number of primary turns
$\qquad\qquad\quad N_{\text{sec}}$ = number of secondary turns

16

By using (10) and (11) (9) becomes

$$P_{\text{winding}} = I_p^2 \sigma_p \frac{l_w N_{\text{prim}}^2}{A_{\text{prim}}} + I_s^2 \sigma_s \frac{l_w N_{\text{sec}}^2}{A_{\text{sec}}}$$

(12)

When magnetizing current is neglected and balanced operation between the windings is assumed the ratio of primary and secondary current is:

$$I_s = I_p \frac{N_{\text{prim}}}{N_{\text{sec}}}$$

(13)

When (total) winding area A_w (see Figure 2 and 3) is used, the ratio of primary winding A_{prim} to (total) winding area A_w is notated as n and the winding fill factor is notated as α and (13) is used (12) becomes:

$$P_{\text{winding}} = I_p^2 \sigma_p \frac{l_w N_{\text{prim}}^2}{n A_w \cdot \alpha} + \left(\frac{N_{\text{prim}}}{N_{\text{sec}}} I_p\right)^2 \sigma_s \frac{l_w N_{\text{sec}}^2}{(1-n) A_w \cdot \alpha}$$

(14)

where $\qquad A_w$ = (total) winding area (m^2)

If the primary and secondary windings have the same unit resistance σ (14) simplifies into:

$$P_{\text{winding}} = I_p^2 \sigma \frac{l_w N_{\text{prim}}^2}{A_w \cdot \alpha} \left\{ \frac{1}{n(1-n)} \right\}$$

(15)

The increase of winding loss with frequency due to skin and proximity effects is usually treated by deriving the values for winding resistance versus frequency, by calculating the loss at each harmonic current component using the obtained winding AC-resistance values and by finally summing the losses at separate harmonics together.

The winding loss caused by load current in terms of material, geometry, excitation and winding implementation parameters is now:

$$P_{\text{winding}} = \sum_{h=0}^{\infty} \sigma \frac{l_w N_{\text{prim}}^2}{A_w \cdot \alpha} \left\{ \frac{1}{n(1-n)} \right\} I_{Ph}^2 \left(\frac{R_{\text{ac}}}{R_{\text{dc}}}\right)_h$$

(16)

where $\qquad I_{ph}$ = primary rms current at h^{th} harmonic frequency
$\qquad\qquad\qquad (R_{\text{ac}}/R_{\text{dc}})_h$ = ratio of AC and DC resistance at h^{th} harmonic frequency
$\qquad\qquad\qquad h$ = index for harmonic components

Winding fill factor α and ratio of primary winding area to total winding area n can be regarded as winding implementation parameters. For optimum transformer $\alpha = 1$ and $n = 0.5$. Winding fill factors of different manufacturing methods are illustrated in Figure 9 below.
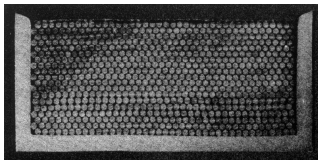
0.19mm enamelled wire
fill factor = 0.93
[38 p. 316]
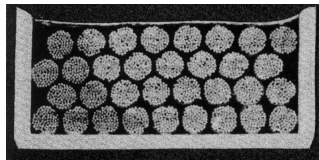
81 x 0.071mm bunched
fill factor = 0.87
[38 p. 316]

Multilayer PCB
fill factor = 0.20

Figure 9: Examples of winding cross sections with various winding methods

Winding implementation parameters can also be determined from a physical prototype by winding DC-resistance measurements :

$$n = \frac{R_{sec} N_{prim}^2}{N_{sec}^2 R_{prim} + R_{sec} N_{prim}^2} \tag{17}$$

$$\alpha = \frac{\sigma l_w N_{sec}^2 R_{prim} + \sigma l_w R_{sec} N_{prim}^2}{R_{prim} R_{sec} A_w} \tag{18}$$

The increase of winding resistance versus frequency (R_{ac}/R_{dc}) due to skin and proximity effects was treated analytically by Dowell [30] and Ferreira [37] with the results applicable to foil and solid round wire windings, respectively. The exact AC-resistance of more complex winding geometries for example with passive windings and static shields can be determined using Finite Element Method (FEM) analysis [7].

The ratio of AC to DC-winding resistance (R_{ac}/R_{dc}) for foil winding is [30]:

$$\frac{R_{ac}}{R_{dc}} = y \left[M(y) + \frac{2}{3}(m^2 - 1) D(y) \right] \tag{19}$$

where

$$y = \frac{d_{foil}}{\delta}$$

d_{foil} = foil thickness (m)

$$\delta = \sqrt{\frac{2}{2\pi f \mu_0 \sigma}}, \text{ skin depth at frequency } f$$

m = number of layers in winding section   (see Figure 12)

$$M(y) = \frac{\sinh(2y) + \sin(2y)}{\cosh(2y) - \cos(2y)}$$

$$D(y) = \frac{\sinh(y) - \sin(y)}{\cosh(y) + \cos(y)}$$

The ratio of AC to DC-winding resistance (R_{ac}/R_{dc}) for solid round wire is [37]:

$$\frac{R_{ac}}{R_{dc}} = \frac{\xi}{2} \left[\frac{\sinh \xi + \sin \xi}{\cosh \xi - \cos \xi} + (2m - 1)^2 \frac{\sinh \xi - \sin \xi}{\cosh \xi + \cos \xi} \right] \tag{20}$$

where

$$\xi = \frac{\sqrt{\pi}}{2} \frac{d_{wire}}{\delta}$$

d_{wire} = wire diameter (m)

$$\delta = \sqrt{\frac{2}{2\pi f \mu_0 \sigma}}, \text{ skin depth at frequency } f$$

Interleaved ($m \sim 1$) foil, multistrand and litz wire windings with conductor diameter near skin depth (y or $\xi \sim 1$) are used in order to reduce high frequency winding losses.

3.4 MAGNETIZING CURRENT WINDING LOSSES

Magnetizing current i_m waveform with no DC-bias component, with switching frequency f and duty cycle D is sketched into Figure 10 below. Constant magnetization inductance L_m has been assumed.
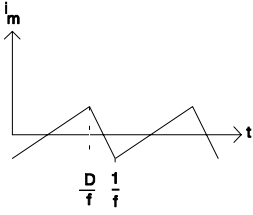

Figure 10: Magnetization current waveform

The winding loss caused by the magnetizing current (Figure 10) in primary winding is calculated by piece-wise integration of instantaneous winding loss ($P = I_m^2 R_{prim}$). DC-winding resistance R_{prim} is assumed.

$$P_m = 2 \cdot \frac{2f}{D} \int_0^{\frac{D}{2f}} R_{prim} \left(\frac{U_{in}t}{L_m} \right)^2 dt + 2 \cdot \frac{1}{\frac{1}{2}\left(\frac{1}{f} - \frac{D}{f} \right)} \int_0^{\frac{1}{2}\left(\frac{1}{f} - \frac{D}{f} \right)} R_{prim} \left(\frac{U_{in}\frac{D}{1-D}t}{L_m} \right)^2 dt \qquad (21)$$

where   Magnetizing inductance $L_m = N_{prim}^2 \dfrac{\mu_0 \mu_r A_c}{l_c}$

                 Primary winding resistance $R_{prim} = \sigma \dfrac{l_w N_{prim}^2}{A_w \alpha n}$

                                  f = (switching) frequency   (Hz)
                                  D = duty cycle   (0 … 1)
                                  U_{in} = input voltage   (V)

(21) becomes:

$$P_m = \frac{R_{prim} U^2 D^2}{3 L_m^2 f^2} \qquad (22)$$

The winding loss caused by transformer magnetizing current is usually considered to be negligible. However, because the magnetization current is inductor - type (i.e. magnetic field of magnetizing current portion of primary current is not cancelled by equivalent secondary ampere-turns) the detailed calculation would require harmonic loss analysis with number of layers per section being the total number of primary layers with secondary layers being considered as passive layers.

3.5 WINDING PARASITICS

Non-ideal magnetic field coupling and non-intended electrical field coupling between primary and secondary windings results leakage inductance and interwinding capacitance, respectively. Capacitance inside both windings themselves (intrawinding capacitance) also exists but it is neglected here. Leakage fields are frequency dependent but in following the leakage inductance and interwinding capacitance are approximated for static DC-fields, only. In order to further simplify analysis the magnetic field is notated to be concentrated into the volume between the windings and not to penetrate within the conductors or exist in region outside the winding (infinite core permeability).

The leakage inductance and interwinding capacitance per unit length (in the direction perpendicular to paper) within the structure of Figure 11 are:

$$L_{layer} = N^2 \frac{\mu_o \mu_r x}{w} \qquad (23)$$

where L_{layer} = Inductance of volume between winding layers (H/m)

19

μ_r = relative permeability
μ_o = permeability of vacuum
N = number of (primary) turns per layer
x = distance between winding layers (m)
w = winding layer width (m)

$$C_{\text{layer}} = \varepsilon_o \varepsilon_r \frac{w}{x} \qquad (24)$$

where C_{layer} = Capacitance between winding layers (F/m)
                 ε_r = relative permittivity
                 ε_o = permittivity of vacuum
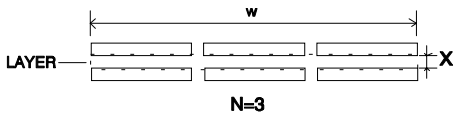
Figure 11: Layer-to-layer interface

A winding section (Figure 12) notates into a one set of primary and secondary winding layers within a winding. When equivalent primary and secondary winding volumes are assumed the leakage inductance per unit length within a section with m (primary) winding layers is:

$$L_{\text{section}} = \frac{\mu_0 \mu_r N^2 m(m^2 + m)x}{w} \qquad (25)$$

where L_{section} = inductance of a section (H/m)
                 m = number of (primary) layers in winding section
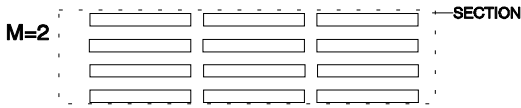
Figure 12: A winding section with 2 layers of primaries and secondaries (m = 2)

The number of sections N_s in total winding (Figure 13) is:

$$N_s = \frac{N_{\text{prim}}}{N \cdot m} \qquad (26)$$

where N_{prim} = total number of primary winding turns

The total leakage inductance L_{total} per unit length within the winding (Figure 13) is now calculated using (23),(25) and (26):

$$L_{\text{total}} = \frac{\mu_0 \mu_r N_{\text{prim}} N(m^2 + m)x}{w} \qquad (27)$$

20
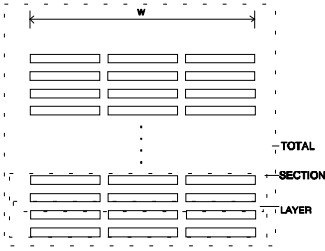
Figure 13: Total winding

Total capacitance between primary and secondary is approximated by multiplying the layer capacitance (24) with the total number of primary to secondary interfaces.

For completely interleaved primary and secondary winding layers (Figure 14) the total capacitance per unit length between primary and secondary windings is:

$$C_{\text{total}} = C_{\text{layer}} \left(2 \cdot \frac{N_{\text{prim}}}{N \cdot m} - 1 \right) \tag{28}$$
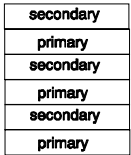
Figure 14: Complete interleaving

For primary and secondary winding layers interleaved in groups of two similar layers except for the outest layers (Figure 15) the total capacitance per unit length between primary and secondary winding layers is:

$$C_{\text{total}} = C_{\text{layer}} \left(\frac{N_{\text{prim}}}{N \cdot m} \right) \tag{29}$$
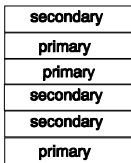
Figure 15: Interleaving in groups of 2 similar layers

The latter interleaving method (29) results approximately half the interwinding capacitance over (28) although both have about the same leakage inductance.

The leakage inductance and interwinding capacitance are also interrelated and in design a compromise between these is needed. The interleaving is typically limited into 4 - 5 times. Static shields between primary and secondary windings can also be considered. Using (29) and (27) the relation between per unit length leakage inductance and interwinding capacitance becomes:

$$L_{\text{total}} = \frac{\mu_0 \mu_r \varepsilon_0 \varepsilon_r N_{\text{prim}}^2 (m+1)}{C_{\text{total}}} \tag{30}$$

21

3.6 TEMPERATURE RISE

Thermal design of electronic components and systems aims to ensure that the temperature rise caused by the losses remains within acceptable limits. Heat transfer mechanisms: *conduction*, *convection* and *radiation* from an object on printed circuit board (PCB) are illustrated in Figure 16.

The heat *conducted* $P_{conduction}$ from the object to printed circuit board (PCB) is:

$$P_{conduction} = R_{th\_obj-PCB}(T_{obj} - T_{PCB}) \tag{31}$$

where $\quad R_{th\_obj-PCB}$ = conductive thermal resistance from object to PCB (K/W)
T_{obj} = object temperature (K)
T_{PCB} = printed circuit board (PCB) temperature (K)

In *convection* the heat is transferred by a moving fluid. Fluid can be moved by temperature difference driven buyonance (*natural convection*) or for example by a fan (*forced convection*). Convective heat transfer capacity includes non-linear heat transfer coefficient β:

$$P_{convection} = \beta A(T_{obj} - T_{amb}) \tag{32}$$

where $\quad \beta$ = convective heat transfer coefficient
A = surface area (m^2)
T_{amb} = ambient temperature (K)

Radiative heat exchange between object and ambient depends on surface emissivity, area and difference of 4th powers of temperatures:

$$P_{radiation} = \sigma_B \varepsilon A(T_{obj}^4 - T_{amb}^4) \tag{33}$$

where $\quad \sigma_B$ = Boltzmann coefficient
ε = emissivity
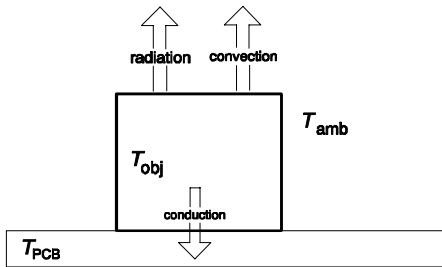
Figure 16: Heat transfer mechanisms from an object on PCB to ambient

Natural convective and *radiative* heat transfer from a cubic object were treated analytically in terms of component dimensions in [39] and [P2].

For *natural convection* the convective heat transfer capacity $P_{convection}$ of a cubic object with dimensions in inches and with no convection through bottom is [P2]:

$$P_{convection} = 2 \cdot 10^{-3} \left[4.6(l_{obj} + w_{obj})h_{obj}^{0.75} + 1.8(l_{obj}w_{obj})^{0.75}(l_{obj} + w_{obj})^{0.25} \right] (T_{obj} - T_{amb})^{1.25} \tag{34}$$

where $\quad l_{obj}$ = length of object (in)
w_{obj} = width of object (in)
h_{obj} = height of object (in)
T_{obj} = object temperature (K)
T_{amb} = ambient temperature (K)

Radiative heat transfer capacity $P_{\text{radiation}}$ of an object with emissivity of 0.85, no radiation through bottom and dimensions in inches is [39]:

$$P_{\text{radiation}} = 3.3 \cdot 10^{-11} \left[(l_{\text{obj}} + w_{\text{obj}})h_{\text{obj}} + l_{\text{obj}}w_{\text{obj}} \right] (T_{\text{obj}}^4 - T_{\text{amb}}^4) \qquad (35)$$

Regression analysis (Figure 17) between calculated (34),(35) and measured total heat transfer capacities (convective and radiative) of cubic thermal test objects show good agreement (y = 1.0028 - 0.0305 : r^2 = 0.9497) between theory and experiments.
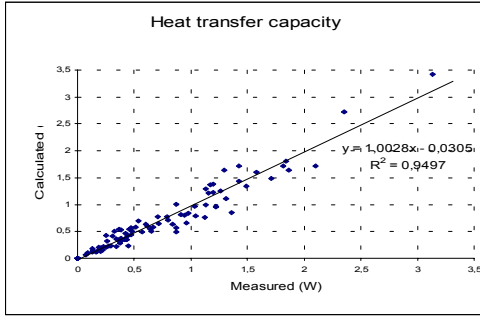
Figure 17: Calculated and measured heat transfer capacity (27),(28) of cubic thermal test objects

The transformer thermal model can also be determined empirically for example by temperature rise measurements with a range of DC-current generated winding and core losses. Candidate empirical thermal model and curve-fit coefficients are shown in Figure 18 with regression analysis between predicted and measured temperature rise values (y = 1.0091x - 0.0201 : r^2 = 0.9891).
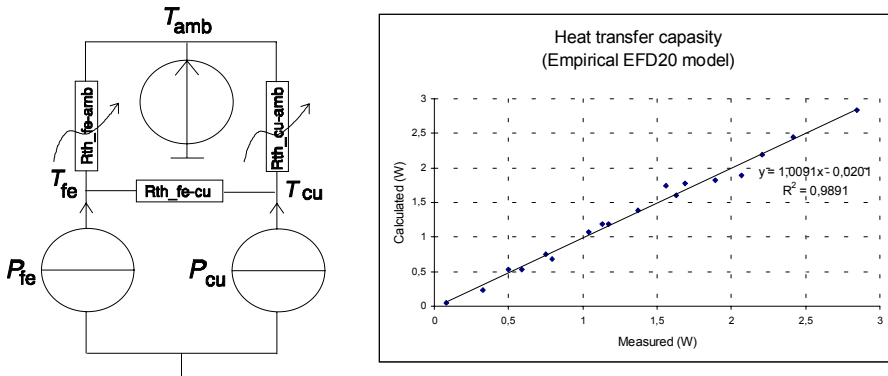
$$P_{\text{fe}} = a_{\text{th}}(T_{\text{fe}} - T_{\text{amb}})^{b_{\text{th}}} + e_{\text{th}}(T_{\text{fe}} - T_{\text{cu}})$$

$$P_{\text{cu}} = c_{\text{th}}(T_{\text{cu}} - T_{\text{amb}})^{d_{\text{th}}} - e_{\text{th}}(T_{\text{fe}} - T_{\text{cu}})$$

a_{th} = 0.0022, b_{th} = 1.4064, c_{th} = 0.0074, d_{th} = 1.1283 and e_{th} = 0.0494.

Figure 18: Empirical EFD20 transformer thermal model [P2]

3.7 POWER TRANSFORMER LOSS AND TEMPERATURE RISE CALCULATION

Separate loss and temperature rise calculations (Table 1) must be linked in order to calculate both transformer losses and temperature rise. The temperature rise can be calculated iteratively by setting the transformer temperature to a value where the total heat transfer capacity of all heat transfer mechanisms (conduction, convection and radiation) equals to the total power loss in the component. Such iterative calculation makes it also easier to take temperature dependency of losses into account.

Table 1: Loss and temperature rise calculations in this work

ISSUE:	MODEL:	PARAMETERS:
Core hysteresis loss	Modified Steinmetz [35]	$K1,K2,K3,ct2,ct1,ct,U_{in},f,D,A_c,l_c$
Core eddy current loss	Bulk resistivity model [34]	$\rho,\ U_{in,}\ f,D,\ A_c,l_c$
Magnetization current winding loss	-	-
Load current winding loss	Dowell & Ferreira Rac/Rdc harmonic analysis [30],[37]	$A_w,l_w,\ n,\alpha,\sigma,R_{ac}/R_{dc},\ U_{in,}\ f,D,\ I_{rms(f)}$
Conductive heat transfer	- / measured	$-/R_{th\_obj\text{-}PCB}$
Convective heat transfer	2 x corrected [39]	l_{obj},w_{obj},h_{obj}
Radiative heat transfer	[39]	l_{obj},w_{obj},h_{obj}

The transformer loss and temperature rise calculation algorithm considered in this thesis [P2] (Figure 19) consists of two loops. The inner sets the transformer temperature to a value where the total heat transfer capacity (30), (31), (32) equals to the total losses in the component. The outer loop then recalculates the losses according to (6),(8),(16) and (22) by using the updated temperature values for core and winding materials.
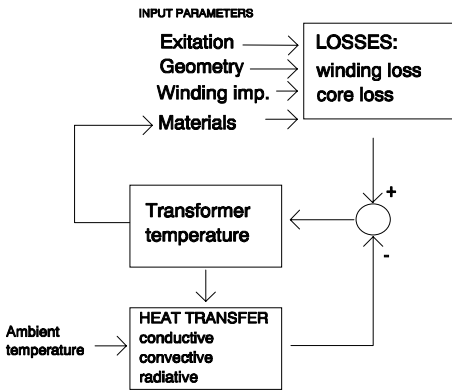
Figure 19: Iterative transformer loss and temperature rise calculation algorithm

Regression analysis between transformer temperature values calculated with the iterative algorithm (Figure 19) using analytical and empirical thermal models and measured in-circuit operation is shown in Figure 20. It can be concluded that the losses are calculated with appropriate accuracy in both cases although the exact temperature rise prediction depends on the availability of conductive heat transfer along interconnections to PCB and other components and is achieved with empirical (estimated) thermal model only.
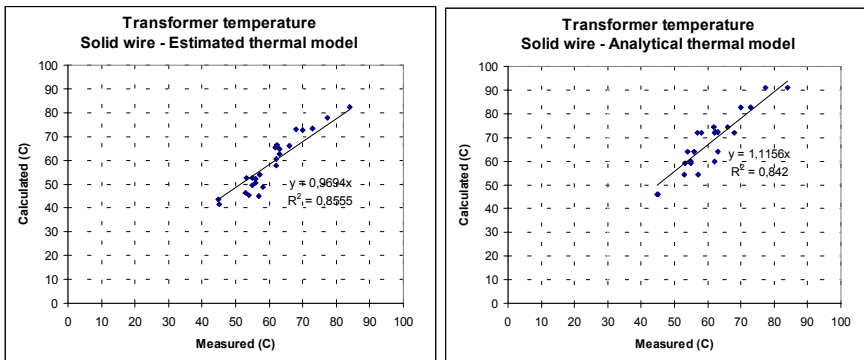
Figure 20: Accuracy of transformer temperature rise calculation

3.8 COST - PERFORMANCE AND DESIGN FOR MANUFACTURING ANALYSIS

By using the notation of this thesis the full custom power transformer design optimization would now seek for the values of A_w, l_w, A_c, l_c and N for excitation U_{in}, f, D, $I_{rms(f)}$ using available winding n, α, σ, R_{ac}/R_{dc} and core $K1$, $K2$, $K3$, $ct2$, $ct1$, ct, ρ technologies in order to satisfy design constraints such as minimum loss, maximum power density or allowed temperature rise. In practical engineering the costs are considered as well. With automatic manufacturing methods the component costs are determined by material costs ($/m^3) and if these are available the designs could be studied for example in terms of losses versus costs as well. For illustration the calculated total losses of Z-folded transformer options are compared versus the main cost driver, the amount of required flexible circuit board area (number of [flex] seqments) in Figure 21. (See Results-chapter and [P7] for details)

Figure 21 Comparison of transformer geometries [P7]
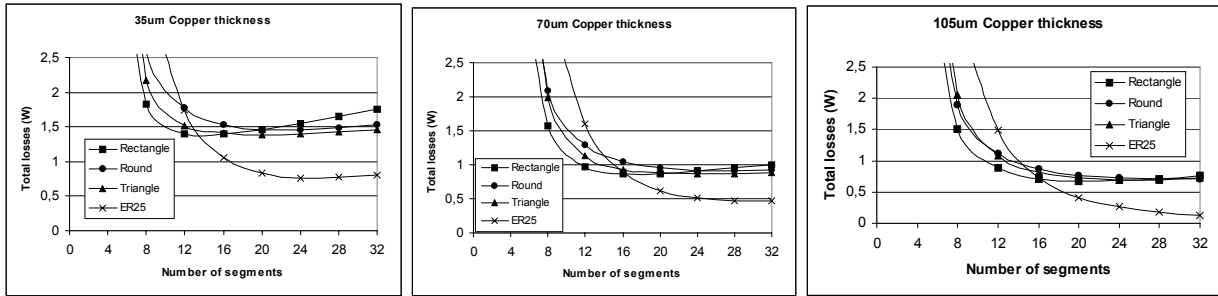
4. SUMMARY OF PUBLICATIONS (RESULTS)

[1] The power density of commercial DC/DC converters was found to increase versus increasing output power only suggesting that these tend to have a fixed (34 cm^3 / 2 inch^3) industry standard minimum volume. On the other hand in journal and conference papers much wider range of power densities have been reported (max. 7.75 W/cm^3 / 130 W/inch^3). Tube-type planar transformer geometry was found to provide more potential for low profile, high power density transformers over disc-type planar transformers. The core length (l_c) thus the volume of disc-type planar increases as the height reduces while the tube-type planar has shorter winding turn length (l_w). For these reasons the latter is preferred in many papers [9], [15] although the disc-type planar is favored in practice perhaps due to manufacturing issues. The power density optimal disc-type design has 60% - 80% copper losses and 40% - 20% core losses while optimal tube-type design has 70% - 50% core losses and 30% - 50% copper losses [9]. Because the material development is obviously reducing the core losses faster than the resistivity of copper (except for superconductors) the tube-type transformer will have even a bigger advantage in the future. A single toroidal core is not suitable for low profile, high power density transformers due to dimensional constraints.

[2] High accuracy (std.error = 0.05W) calorimetric measurements proved that the modified Steinmetz equation and bulk eddy current calculations resulted very accurate core loss predictions (std.error = 0.0581W) across the frequency (100 - 300kHz) and flux density range (0.05 - 0.3T) of interest. Analytical winding AC-resistance equations were validated with FEM analysis and found to provide appropriate accuracy for the practical design purposes. Thermal test block tests suggested a slight modification (multiplier 2 x) for analytical convective heat transfer equation from the literature [39]. After this a good match (r^2 = 0.95) was achieved between calculated and measured heat transfer capacities with a standard error of 0.15W across the loss range of 0 - 2W. An empirical thermal model resulted slightly smaller heat transfer capacity standard error (0.0834W). Losses in interconnecting wires was the biggest uncertainty of in-circuit transformer temperature rise estimations even though the transformers were not of a high current single turn secondary type. Results obtained by using the corrected (2 x) analytical thermal model were almost as accurate as with the estimated EFD20 thermal model due to relatively small (15 - 25%) heat conduction through interconnection wires. The results suggest that the transformer total losses can be predicted with the average standard error below 0.2W with datasheet type information only. Further, if conductive thermal resistance from transformer via printed circuit board substrate to ambient is available the transformer operating temperature could be predicted with appropriate accuracy (5.6ºC) as well.

[3] Thermal resistance from surface mounted component on each Printed Circuit Board to ambient varied from 58.7 K/W (1-layer FR4 0.38$) to 7.9 K/W (2-layer IMS 2.15$) corresponding to approximately 2.7 times difference in throughput power for the same (100 K) temperature rise when resistive-type ($P = I^2R$) losses are assumed. 1-layer IMS and 2-layer 0.1mm FR4 boards with thermally conducting insulator between board and enclosure had only slightly higher thermal resistance than the versions mounted directly against the enclosure (2-layer IMS and 1-layer 0.1mm FR4) obviously due to large effective contact area provided by flexible insulator.

[4] The static shield only and both static shield and windings were successfully deposited and etched directly on the toroidal NiZn core. In latter case the Finite Element Method (FEM) analysis suggests 4.125 times lower capacitance between winding turns and also 5.22 times higher capacitance to static shield than to the next winding turn. This and the adequate high frequency core permeability resulted transfer loss resonant frequency to be as high as 1.2GHz.

[5] Multilayer foil winding with interleaved primary and secondary layers was successfully implemented for EFD30-type transformer using the new manufacturing method. The leakage inductance of the proposed winding method was less than 10% of the value achieved using a wire-wound winding with a single secondary winding between 2 primary layers. The increase of winding losses with wire-wound version was 6.2 times higher than with the proposed winding method across the frequency range of 100kHz - 1.6MHz. The results also show a good agreement between calculated, FEM derived and measured winding AC-resistance values.

[6] New winding layout principles for Z-folded inductive components were developed. As a result a single sided flexible circuit board (FLEX) can be used in manufacturing in order to reduce material costs and to make level of interleaving between primary and secondary windings adjustable. Cost-performance analysis suggests 3 - 5 times better figure-of-merit (Winding DC conductance / total material costs) over multilayer PCB planar transformers. Various Z-folded concepts can be sorted resulting an order of preference as: improved helical, spiral with 1 turn per layer, spiral with 2 turns per layer, spiral with 3 turns per layer, 3 pole, spiral with 4… turns, etc. Copper thickness doubling and adjacent FLEX face via forming worked as expected. Interleaving studies with 3-pole transformer resulted leakage inductance and interwinding capacitance ranges of 987nH to 270nH and 19pF to 103pF, respectively.

[7] Manufacturability and electrical performance of 1- and 2-pole z-folded transformers were compared. The 1-pole (ER25) core with widest conductor resulted lowest total losses. With 2-pole transformers the minimum losses for the same maximum dimensions were about double. However, the 2-pole transformers achieved their minimum loss range with the least number of FLEX segments because they build up turns quicker to reduce core losses and may be preferred when cost – performance is considered. From 2-pole options the rectangular pole has lowest losses for given number of segments obviously because the optimization constraints (component dimensions) were in rectangular coordinates as well. Measurements with prototype transformers suggest that the analytical relation between interwinding capacitance and leakage inductance is valid and that the parasitics might be predicted with a reasonable accuracy if some characterization measurements such as effective permeability and distance between primary and secondary layers would be done prior to design. In appendix 1 it is shown that core geometries with more than 1 pole pairs suffer from excessive core losses when constant total core cross sectional area is considered.

5. CONCLUSION

According to the results it can be concluded that both aims of the work were met:

- A high frequency power transformer *design algorithm* was successfully developed, implemented into a spreadsheet and validated using regression analysis between predicted and measured in-circuit temperature rise values.

- Improved, mass manufacturable winding *implementation methods* were developed for toroidal, tube-type planar and disc-type planar high frequency power transformers and validated by calculations, simulations and measurements.

6. DISCUSSION

The new winding methods successfully developed for toroidal, tube-type and disc-type planar transformer geometries have potential for mass manufacturing of power transformers and other inductive components as well. However, the prototype transformers used for illustrating the new winding concepts were quite far from optimum designs and implementations. For example in [P4] the standard toroidal core geometry with thin single layer conductors resulted a considerably low copper fill factor. Oval core geometry and multilayer windings maybe based on photo definable epoxies and photo definable additive copper plating processes might have result copper fill factor required by high power density power transformers. In [P5] 80μm polyester / 20μm copper laminate was used for winding due to availability reasons resulting considerably winding DC-resistance (primary = 7.7Ω) as well. On the other hand it is obvious that such a high DC resistance level made AC resistance determination using 50Ω generator, shunt resistor and digital oscilloscope possible. In later studies with mΩ winding DC resistance values this method didn't give reliable results.

To the authors best knowledge [P2] is the first published study on high frequency power transformer design where core and winding losses are combined with thermal models and validated successfully in circuit operation using statistical methods and can be regarded as the main scientific contribution of the thesis. The analytical convective and radiative thermal models, estimation of thermal model using DC-generated core losses and combined loss and thermal calculation spreadsheet can be regarded as particularly useful results. The use of regression analysis to validate each and all design issues proved to be very efficient in providing confidence and eliminating possible errors in models, parameter values and calculation spreadsheet. Such quantitative methods to compare design calculations and actual measurements have been used quite seldom in electrical engineering literature. It can be concluded that the developed transformer design procedure itself provides an appropriate method to predict transformer core and winding losses and resulting temperature rise but the availability of material loss parameters and conductive thermal resistance from transformer to printed circuit board (PCB) may become a practical problem. The good correlation between calculated and measured values was in some extend result of a simple core and winding geometries. For lower profile planar transformers the current and flux crowding should be taken into account by 2D/3D FEM analysis and measurements based correction factors. R_{ac}/R_{dc}-functions for more complex winding geometries and converter topologies should also be developed using FEM analysis and impedance analyzer measurements. On the other hand it might be more beneficial to develop winding geometries with R_{ac}/R_{dc} (f) ~1 using these methods in the first place. The effect of DC-bias on core losses should also be taken into account in particular for inductor design. Transformer parasitics (leakage inductance, inter- and intrawinding capacitance) were not treated adequately. The losses caused by these are inflicted mainly into switching components while the interwinding capacitance contributes to the electromagnetic interference (EMI) as well. These should be considered in the converter level design analysis which was not within the scope of this thesis. Although the design equations developed in this work may be valid for power transformers with similar operational conditions and comparable dimensions only the idea of developing design equations for losses and heat transfer first by analytical, numerical or empirical means and by then combining these for design analysis may be expanded to design optimization of other inductive components and power converters as well. For practical engineering the most important issue is often the cost - performance obtainable with different manufacturing methods and design optimization algorithms. However, the manufacturing and material costs are not often considered in literature. This is obviously due to non-availability and confidentiality of cost information. In this work a quantitative cost - performance analysis was considered only briefly in [P7] and (3.8). However, the design spreadsheet of [P2] could be quite easily upgraded to include material costs in order to provide similar analysis for practical transformer design optimization as well.

7. REFERENCES

[1] Ridley R.B., Zhou C., Lee F.C., "Application of Nonlinear Design Optimization for Power Converter Components", *IEEE Transactions on Power Electronics*, vol. 5, No. 1, Jan 1990

[2] Callander G., Garnier A., Johnson S., "Analytical Minimal Loss Design of Transformers for High Frequency Switch Mode Convertors", *Proc. Tenth Annual IEEE Applied Power Electronics Conference*, vol. 1, pp. 361 – 366, 1995

[3] Petkov, R., "Optimum design of a high-power, high-frequency transformer", *IEEE Transactions on Power Electronics*, vol. 11, no. 1, pp. 33 – 42, Jan 1996

[4] Hurley, W.G., Wolfe, W.H., Breslin, J.G., "Optimized transformer design: inclusive of high-frequency effects", *IEEE Transactions on Power Electronics*, vol. 13, no. 4, pp. 651-659, Jul 1998

[5] Gradzki P.M., Jovanovic M.M., Lee F.C., "Computer-aided Design for High-frequency Power Transformers", *Proc. Fifth Annual IEEE Applied Power Electronics Conference*, pp. 336 – 343, 1990

[6] Apeldoorn O., Kriegel K., "Optimal Design of Transformers for High-power High Frequency Applications", EPE'95, 1995

[7] Robert F., Mathys P., "A closed-form Formula for 2D Ohmic losses Calculation in SMPS Transformer Foils", *Proc. 14th Annual IEEE Applied Power Electronics Conference*, vol. 1, pp. 199 – 205, 1999

[8] Imre T.G., Cronje W.A., van Wyk J.D., Ferreira J.A., "Experimental Validation of Loss Calculations for a Planar Inductor", *Proc. IEEE 30th Annual Power Electronics Specialists Conference*, vol. 1, pp. 586 – 591, 1999

[9] Ramakrishnan S., Steigerwald R.L., Mallick J.A., "A Comparison Study Of Low-profile Power Magnetics For High-frequency, High-density Switching Converters", *Proc. 12th Annual IEEE Applied Power Electronics Conference and Exposition, vol.1,* pp. 388 - 394, 1997.

[10] Hofsajer I.W., van Wyk J.D., Ferreira J.A., "Volume considerations of planar integrated Components", *Proc. IEEE 30th Annual Power Electronics Specialists Conference*, vol.2, pp. 741 - 745, 1999

[11] Goldberg A.F.,Schlecht M.F., "The Relationship Between Size and Power Dissipation in a 1 - 10 MHz Transformer", *Proc. IEEE 20th Annual Power Electronics Specialists Conference*, vol.2, pp. 625 - 634, 1989

[12] Ngo K.D.T., Lai R.S.,"Effect of Height on Power Density in high-frequency transformers", *Proc. IEEE 22nd Annual Power Electronics Specialists Conference*, pp. 667 – 672, 1991

[13] Ngo K.D.T., Alley Robert P., Yerman A.J., Charles R.J., Kuo M.H., "Design Issues for the Transformer in a Low-voltage Power Supply with High Efficiency and High Power Density", *IEEE Transactions on Power Electronics*, vol.7, no. 3, July 1992

[14] Gu W., Liu R., "A Study of Volume and Weight vs. Frequency for High-Frequency Transformers", *Proc. IEEE 24th Annual Power Electronics Specialists Conference*, pp. 1123 - 1129, 1993

[15] Katane T., Nohgi H., Sakaki Y., "Optimum Core Dimensions of Transformer for Switching Power Supplies", *Proc. IEEE 25th Annual Power Electronics Specialists Conference*, vol.1, pp. 24 - 28, 1994

[16] Hurley W.G., Gath E., Breslin J.G., "Optimizing the AC resistance of multilayer transformer windings with arbitrary current waveforms", *IEEE Transactions on Power Electronics,* vol. 15, no. 2, March 2000

[17] Quinn C., Rinne K., O'Donnell T., Duffy M., Mathuna C., "A Review of Planar Magnetic Techniques and Technologies", *Proc. 16th Annual IEEE Applied Power Electronics Conference*, vol.2., pp. 1175 - 1183, 2001

[18] Prieto R., Cobos J. A., Garcia 0.) Alou P., Uceda J., "Taking Into Account All The Parasitic Effects In The Design Of Magnetic Components", *Proc. 13th Annual IEEE Applied Power Electronics Conference and Exposition,* vol. 1, pp. 400 - 406, 1998.

[19] Henze C.P., "Electric Vehicle Charger with Printed Circuit Board Magnetic Components", *Proceedings of 15th Annual IEEE Applied Power Electronics Conference and Exposition*, vol. 2, 6 - 10 February 2000, New Orleans, Louisiana

[20] Dai N., Lofti A. W., Skutt G., Tabisz W., Lee F.C., "A comparative study of high-frequency, low-profile planar transformer technologies", *Proc. 9th Annual IEEE Applied Power Electronics Conference and Exposition, vol. 1,* pp. 226 - 232, 1994.

[21] Ngo K.D.T., Alley R.P., Yerman A.J., "Fabrication Method for a Winding Assembly with a Large Number of Planar Layers", *IEEE Transactions on Power Electronics*, vol. 8, no. 1, January 1993

[22] Hu Y-Q., Cheng D. K-W., Lee Y-S., "New Fabrication Method For Planar Multilayer Windings Used In Low-profile Magnetic Components", *IEEE Transactions on Magnetics,* vol. 35, no.2, March 1999.

[23] Lopera J.M., Prieto M.J., Pernia A.M., Nuno F., de Graaf M.J.M., Waanders J.W., Barcia L.A., "Design of Integrated Magnetic Elements Using Thick-film Technology", *IEEE Transactions on Power Electronics*, vol. 14, no.3, May 1999

[24] Duffy M., O'Reilly S., O'Donnell T., Friesen P., McCloskey P., Mathuna S.C.O., "MCM-L Integrated Transformers for Low Power Applications", *Proc. IEEE 31st Annual Power Electronics Specialists Conference*, vol.1, pp. 302 - 307, 2000

[25] Sullivan C.R, Sanders S.R., "Design of Microfabricated Transformers and Inductors for High-Frequency Power Conversion", *IEEE Transactions on Power Electronics*, vol.11, no. 2, March 1996

[26] Lofti A., Van Dover R.B., Schneemeyer L., Steigerwald M., "Micro-transformer Devices Using Thin-film Electroplated deposition", *Proc. IEEE 29th Annual Power Electronics Specialists Conference*, vol. 2, pp. 1511 - 1515, 1998

[27] Sullivan C.R., Sanders S.R., "Measured Performance of a High-power density Microfabricated Transformer in a DC-DC Converter", *Proc. of 27th Annual IEEE Power Electronics Specialists Conference*, vol.1, pp. 287 - 294, 1996

[28] Korman C.S., Ramakrishnan S., Steigerwald R.L., Fisher R.A., Hennessy W., Bicknell W., Wojnarowski R., "Low Profile DC-DC Power Converter for 3-D Electronics Assembly" *Proc. 16th Digital Avionics Systems Conference,* vol. 1, pp. 2.3 - 21.6, 1997.

[29] Reinert J., Brockmeyer A., De Doncker R.W.A.A., "Calculation of Losses in Ferro- and Ferrimagnetic Materials Based on the Modified Steinmetz Equation", *IEEE Transactions on Industry Applications*, vol.37, no.4, Jul/Aug 2001

[30] Dowell P.L., "Effect of eddy currents in transformer windings", *IEE Proc.*, vol. 113, no. 8, pp. 1387 – 1394, Aug. 1966

[31] Goldman A. "Modern Ferrite Technology", Van Nostrand Reinhold, New York, 1990, p. 45 - 66

[32] Knowles J.E., "The Origin of the Increase in Magnetic Loss Induced by Machining Ferrites", *IEEE Transactions on Magnetics*, vol. 11, no.1, Jan 1975, pp. 44 - 50

[33], R.D.Gomez, Domain Wall Motion of Small Permalloy Elements, http://www.ee.umd.edu/~rdgomez/permalloy.htm

[34] Mulder S., "Loss formulas for power ferrites and their use in transformer design", Philips, Eindhoven, 1994

[35] Albach M, Duerbaum T., Brockmeyer A., "Calculating core losses in transformers for arbitrary magnetizing currents a comparison of different approaches" , *Proc. 27th Annual IEEE Applied Power Electronics Conference*, vol. 2, pp. 1463 – 1468, 1996

[36] Roshen W., "Ferrite Core Loss for Power Magnetic Components Design", *IEEE Transactions on Magnetics*, vol.27, no. 6, Nov 1991

[37] Ferreira J.A., "Improved Analytical Modeling of Conductive Losses in Magnetic Components", *IEEE Transactions on Power Electronics*, vol. 9, no. 1, January 1994

[38] E.C. Snelling, "Soft Ferrites - properties and applications", Second Edition, Butterworths, 1988

[39] Zhang, M.T.; Jovanovic, M.M.; Lee, F.C., "Design and analysis of thermal management for high-power-density converters in sealed enclosures", *Proc. 12th Annual IEEE Applied Power Electronics Conference and Exposition*, vol. 1, pp. 405 – 412, 1997